Prediction of the backflow and recovery regions in the backward facing step at various Reynolds numbers

By V. Michelassi[1], P. A. Durbin[2] AND N. N. Mansour[3]

A four-equation model of turbulence is applied to the numerical simulation of flows with massive separation induced by a sudden expansion. The model constants are a function of the flow parameters, and two different formulations for these functions are tested. The results are compared with experimental data for a high Reynolds-number case and with experimental and DNS data for a low Reynolds-number case. The computations prove that the recovery region downstream of the massive separation is properly modeled only for the high Re case. The problems in this case stem from the gradient diffusion hypothesis, which underestimates the turbulent diffusion.

1. Introduction

The Reynolds Averaged Navier Stokes equations (RANS) equations need a turbulence model for computation of Reynolds stresses that stem from averaging the non-linear convective terms. A large family of turbulence models exists in the literature. The models range from simple algebraic expressions for the eddy viscosity to more elaborate formulations which introduce a separate transport equation for each component of the Reynolds Stress tensor. Eddy viscosity models such as the $k-\epsilon$ model still represent a good compromise between accuracy and computational efficiency and will be the subject of this investigation. Moreover, the results of a recent workshop (Rodi *et al.*, 1995) showed that, even though full Reynolds stress models bring more *physics* into the model, the large increment in the computational effort associated with these models is not always followed by a proportional improvement in the quality of the predictions.

Two-equation models of turbulence have been recently tuned with the aid of Direct Numerical Simulation (DNS) data (see *e.g.* Michelassi and Shih, 1991, Rodi *et al.*, 1993). This tuning was mostly done to allow modeling of the near wall region and to reproduce the profiles of the turbulent kinetic energy, k, and of the dissipation rate ϵ in this critical flow region. The tuning was done by using fully developed or turbulent boundary layer flows (Rodi and Mansour, 1990). Most of the so called "low Reynolds number modifications" (LR) to the two-equation models of

1 University of Florence Energetics Department, Italy
2 Stanford University
3 NASA Ames Research Center

turbulence were able to improve the model capability in the flow layer close to the wall. Nevertheless, little or no change at all was found in the core region of the flow since most of the modifications were designed to vanish away from solid boundaries (Zhu and Shih, 1993).

The LR models, which allow the integration of the equations in the near wall region, can successfully model a wide range of flows, but often do not allow flows with strong adverse pressure gradients and/or separation to be computed accurately. This seems to be a general problem associated with the two-equation formulation irrespective of the treatment of the near-wall region (Michelassi, 1993). In the backward facing step flow, both an adverse pressure gradient and flow separation are to be modeled, which makes this test case particularly challenging.

Durbin (1995) computed the backward facing step flow at different Reynolds numbers. His computations proved that downstream of the reattachment point the computed velocity profiles tend too slowly to a boundary layer profile for the high Reynolds number case, but not for the low Reynolds number case. A similar failure was encountered by Rodi (1991) with a two-layer model of turbulence. Again, the velocity profiles in the recovery region tend too slowly to a developed profile. Durbin and Rodi use forms of the two-equation $k-\epsilon$ model which, while based on the Boussinesq assumption, have very little in common with the treatment. This indicates that the problems are stemming from the $k-\epsilon$ frame and not from the wall treatment.

This phenomenon is also of great importance in practical flows with engineering relevance such as the flow in turbomachines. In fact, immediately downstream of the trailing edge of a turbine or a compressor blade, two counterrotating vortices interact with the wake in a very similar manner to that found for the backward facing step. The modeling of the wake downstream of the two vortices is of primary importance in turbomachinery flows because of its impact on the stator-rotor interaction. In this case, the computed wake decay, which is similar to the flow recovery region in the backward facing step, seems to be too slow compared to the measurements as indicated by a number of computations for subsonic and transonic turbines (Michelassi *et al.* 1995). These results were shown to be true regardless of the assumption of a fully turbulent or transitional boundary layer along the blade profile. In the turbomachinery flow case, it is not clear if the discrepancies are due to the inherently unsteady nature of the experimental flow field, or to deficiencies in the model as in the backward facing step where the steadiness of the flow is not an issue.

Although the *recovery region problem* with computing the backstep has been often pointed out, very little has been done so far to identify the causes of the slow recovery downstream of the reattachment point. Two-equation models are known to have theoretical limitations which stem mainly from the eddy viscosity assumption. Still, the ability of these simple turbulence models to mimic a flow with massive separation and the wake decay needs to be improved.

With this in mind three different backward facing step data sets are used to compare with the computations and to identify the reasons for the discrepancies

between computations and measurements in the recovery region.

2. The turbulence model

The turbulence model uses the standard $k-\varepsilon$ equations:

$$\partial_t k + U \cdot \nabla k = P_k - \varepsilon + [(\nu + \frac{\nu_t}{\sigma_k})\nabla k], \tag{1}$$

$$\partial_t \varepsilon + U \cdot \nabla \varepsilon = \frac{C_{\epsilon 1} P_k - C_{\epsilon 2}\varepsilon}{T} + [(\nu + \frac{\nu_t}{\sigma_\epsilon})\nabla \varepsilon]. \tag{2}$$

The model constant $C_{\epsilon 1}$ is computed as:

$$C_{\epsilon 1} = 1.3 + \frac{0.25}{(1+(d/2L)^2)^4}, \tag{3}$$

in which d is the minimum distance from the wall, and L is the turbulence length scale. On no-slip boundaries, $y \to 0$,

$$k = 0, \ \epsilon \to 2\nu \frac{k}{y^2}.$$

Two additional equations are solved. The first transport equation determines the velocity fluctuation normal to the wall, $\overline{v^2}$. The $\overline{v^2}$ transport equation is

$$\partial_t \overline{v^2} + U \cdot \nabla \overline{v^2} = kf - \overline{v^2}\frac{\varepsilon}{k} + \nabla \cdot [(\nu + \nu_t)\nabla \overline{v^2}], \tag{4}$$

where kf represents redistribution of turbulence energy from the streamwise component. Non-locality is represented by solving an elliptic relaxation equation for f:

$$L^2 \nabla^2 f - f = \frac{C_1 - 1}{T}\left[\frac{\overline{v^2}}{k} - \frac{2}{3}\right] - C_2 \frac{P_k}{k}, \tag{5}$$

in which

$$T = \max\left[\frac{k}{\varepsilon}, 6\left(\frac{\nu}{\varepsilon}\right)^{1/2}\right], \ L = C_L \max\left[\frac{k^{3/2}}{\varepsilon}, C_\eta \left(\frac{\nu^3}{\varepsilon}\right)^{1/4}\right]. \tag{6}$$

The Boussinesq approximation is used for the stress-strain relation:

$$a_{ij} = \frac{\overline{u_i u_j}}{k} - \frac{2}{3}\delta_{ij} = -\frac{\nu_t}{k} S_{ij},$$

where the eddy viscosity is given by

$$\nu_t = C_\mu \overline{v^2} T.$$

The constants of the model are:

$$C_\mu = 0.19,\ \sigma_k = 1,\ \sigma_\epsilon = 1.3, C_{\epsilon 1} = 1.55,\ C_{\epsilon 2} = 1.9$$

$$C_1 = 1.4,\ C_2 = 0.3,\ C_L = 0.3,\ C_\eta = 70. \tag{7}$$

The boundary conditions are

$$\overline{v^2} = 0,\ f(0) \to -\frac{20\nu^2\overline{v^2}}{\varepsilon(0)y^4}.$$

on no-slip walls.

The original model formulation was modified by Durbin and Laurence (1996) in the expressions for the length and time scales, L and T, and the definition of the model constant $C_{\epsilon 1}$. The length and time scales are now computed to allow a smoother switch from the core-flow values to the near-wall values as follows:

$$L^2 = C_p^2 \left(k^3/\epsilon^2 + C_\eta^2 \nu^{3/2}/\epsilon^{1/2}\right),\ T^2 = k^2/\epsilon^2 + C_T^2 \nu/\epsilon \tag{8}$$

The selected values of the constants are $C_p = 0.2$, $C_\eta = 70$, and $C_T = 6$.

In Eq. (3) the scaling of $C_{\epsilon 1}$ in the near wall region is done by using the wall distance y. The definition of the wall distance can be problematic in complex flows so that Durbin and Laurence (1996) replaced Eq. (3) with another expression based on $\overline{v^2}$ which is suited to feel the proximity of the wall:

$$C_{\epsilon 1} = 1.44\left(1 + 1/30(k/\overline{v^2})^{1/2}\right), \tag{9}$$

This expression, like the one in Eq. (3), is supposed to increase the production of dissipation in the near wall region, where $\overline{v^2}$ goes to zero faster than k. Both the original formulation, hereafter referred as form (1) of the model, and the modified formulation, hereafter referred as form (2), have been applied with the same inlet and boundary conditions.

3. The data sets and the computations

The turbulence model with the two different forms described in the previous section was applied to the computation of three different backward-facing step geometries and different Reynolds numbers.

The first experimental data set considered here is that of Driver and Seegmiller (DS) (1985) which allowed testing the model in a high Reynolds-number configuration with a Reynolds number based on the step height of $37,500$. Measurements were taken by using laser velocimetry and include mean and instantaneous quantities and triple correlations.

The low Reynolds-number case refers to the measurements by Kasagi and Matsunaga (KM) (1995). In this case the flow Reynolds number, based again on the

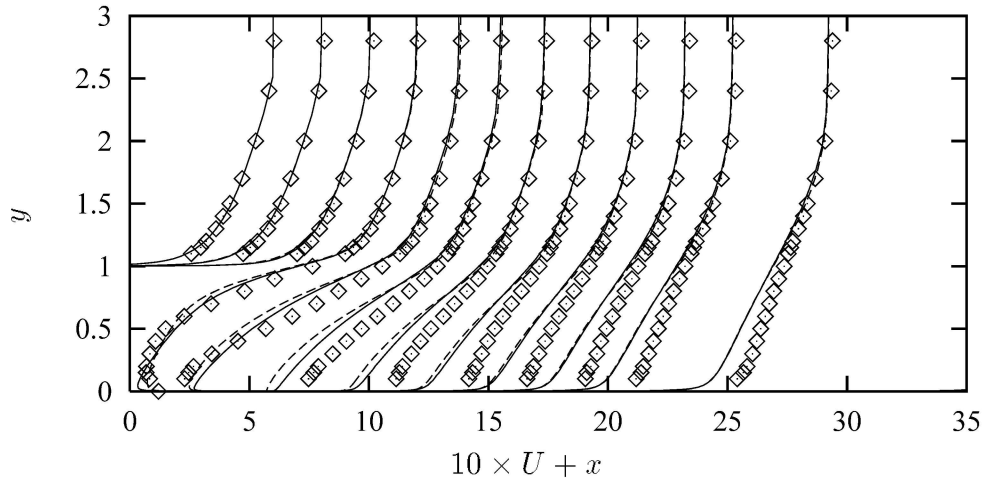

FIGURE 1. *DS* Velocity profiles. ◇ experiments, —— model version (1), – – – model version (2).

step height, is 5540. Measurements were taken by using a particle image velocimetry method (PIV) which allowed measuring instantaneous and average quantities. The measured profiles were also carefully tested to verify mass conservation. A similar Reynolds number ($Re = 5100$) was achieved by Le and Moin (LM) (1994) which produced a DNS data set for the backward facing step geometry. The large amount of information on the flow field makes this DNS data set very valuable for testing and developing two-equation models of turbulence.

The investigation is carried out on three different data sets to test the model under different Reynolds number conditions. At the present stage of research it is still impossible to perform the DNS of a backward facing step at high Reynolds number, so the use of an experimental data set was compulsory. The two data sets for the low Reynolds number case were selected to verify that model testing done by using a classical experimental data set could be extended to the DNS data for such a flow field.

The computational grids for the three test cases have 120×120 grid nodes clustered near solid walls. The inlet section profiles have been carefully specified as follows. For the DS case the inlet profiles have been computed by a boundary layer code until the momentum thickness of 5000 was reached (Durbin, 1995). These profiles were then imposed at the inlet section of the computational domain. For the KM case the inlet profiles were those of a fully developed channel flow, as indicated by Kasagi and Matsunaga (1995) in their discussion of the flow nature upstream of the separation point. For the test case proposed by Le and Moin, the inlet profiles were those computed by the DNS at the section upstream of the separation point corresponding to the inlet section of the present computational grid. No other grids were used for the calculations since the 120×120 grid was already found adequate for this kind of computation by Durbin (1995).

The first set of computations refer to the DS case. Fig. 1 compares the measured profiles with those computed by using the two versions of the model. In all the

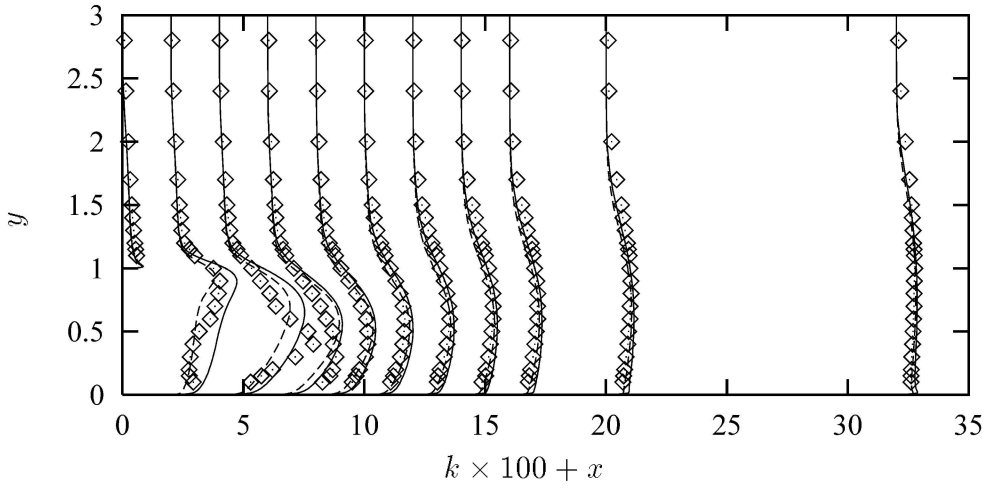

FIGURE 2. *DS* Turbulent kinetic energy profiles. Symbols as in Fig. 1.

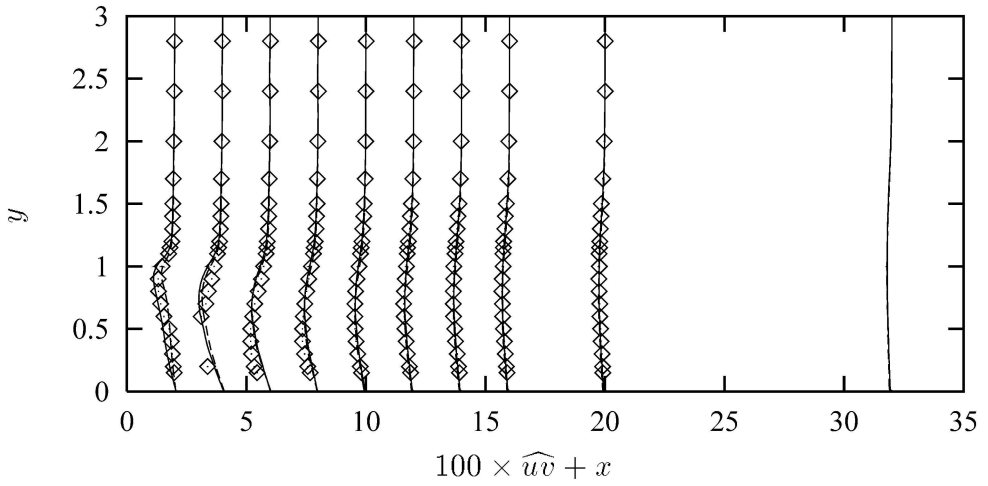

FIGURE 3. *DS* Turbulent shear stress profiles. Symbols as in Fig. 1.

following plots the ordinate $y = 1$ corresponds to the step corner. The reattachment point is not affected by the change in the model, but the different functions adopted for the computation of the length scale L, the time scale T, and the coefficient of the production rate of dissipation $C_{\epsilon 1}$ show some effect in the backflow region. Here version (2) of the model moves the computed profiles closer to experiments. A sensitivity analysis made by changing the coefficients in Eqs. (8, 9) proved that the model is sensitive to the value of C_p, which was set equal to 0.2. The model can be seen to predict velocity profiles which are steeper than the measured ones in the backflow region. Moreover, in the recovery region the computations lag behind the experimental boundary layer profile. The agreement is indeed quite good in terms of turbulent kinetic energy (see Fig. 2) and turbulent shear stress (see Fig. 3). Apparently, the models succeed in reproducing the correct level of turbulent kinetic energy and shear stress with the only exception of a narrow region deep inside of the backflow, where the maximum of turbulent kinetic energy and turbulent shear stress are not correctly predicted and somewhat misplaced.

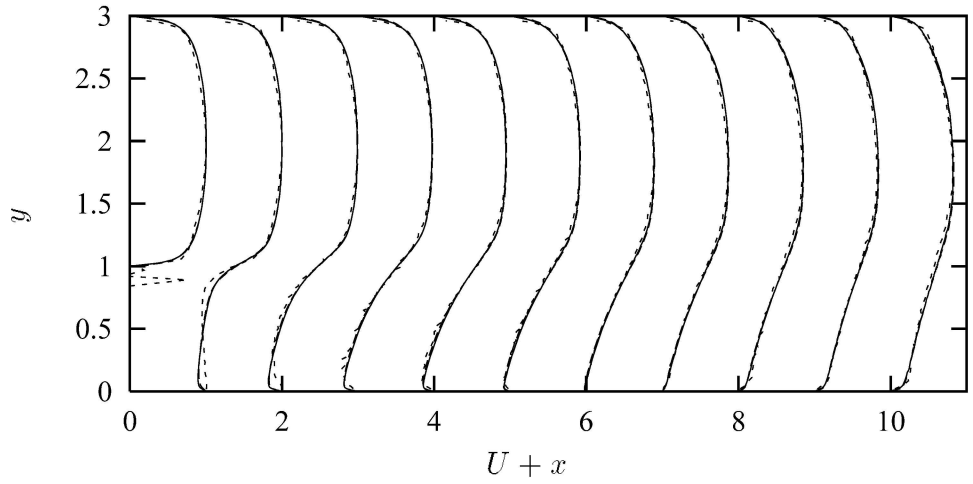

FIGURE 4. *KM* Velocity profiles. ---- experiments, —— model version (1), ——— model version (2).

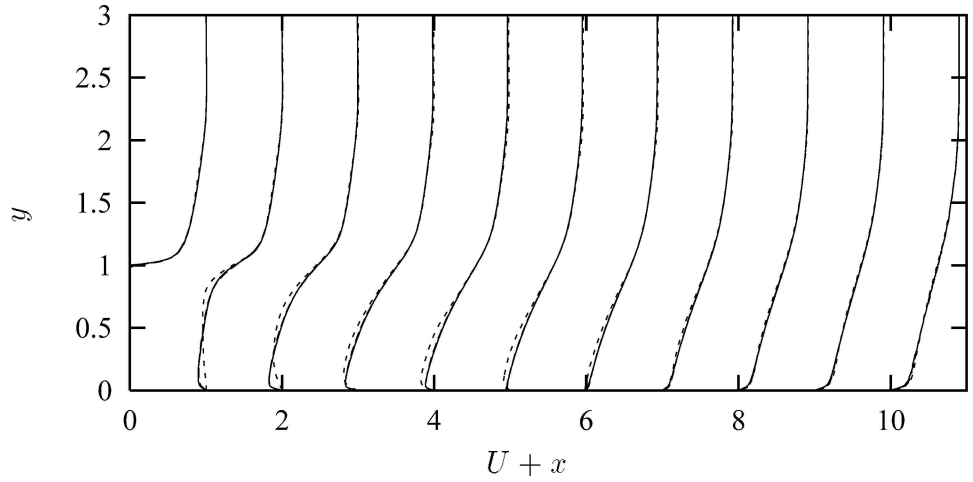

FIGURE 5. *LM* Velocity profiles. Symbols as in Fig. 4.

When moving to the *KM* and *LM* test cases, a more careful analysis is possible due to the large number of measurements. Figure 4 compares the measured and computed velocity profiles in several stations starting from the separation point for the *KM* test case. The agreement is again quite good, and apparently the two versions of the model give almost identical results in this case. The recovery region is well predicted here. Again, the backflow region shows the steep velocity profiles predicted in the high Reynolds number case, while the experiments show a profile which seems to indicate quite a low turbulence level. Figure 5 shows the same velocity profiles for the *LM* test case. In this last computation the recirculation bubble length was underestimated by approximately 4%. The backflow region length was computed in almost perfect agreement with the experiments for the *KM* case. The plots also show that the differences in the computation of the length and time scales in the two versions of the code bring very little change to the computed profiles, which are almost collapsing on each other, in the low Re case.

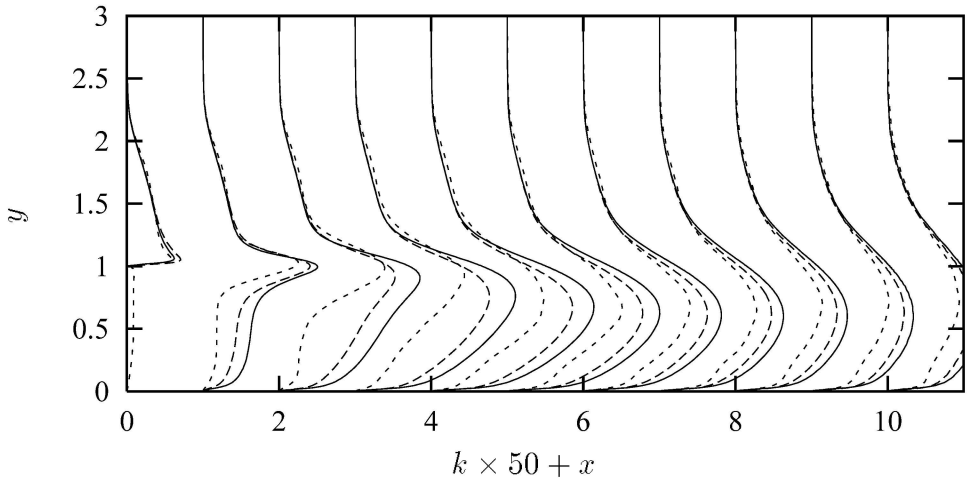

FIGURE 6. *LM* Turbulent kinetic energy profiles. Symbols as in Fig. 4.

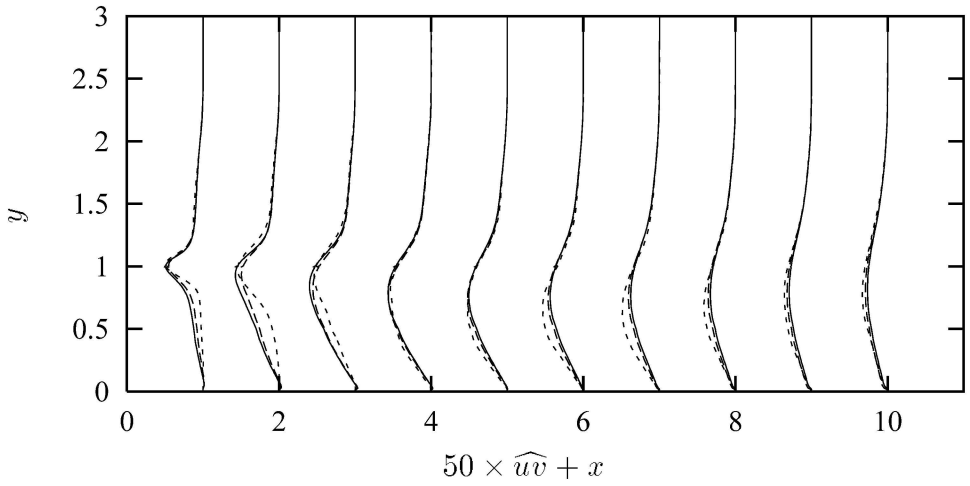

FIGURE 7. *LM* Turbulent shear stress profiles. Symbols as in Fig. 4.

Figures 4 and 5 show that there is very little difference between the LM and KM data sets. Since the information given by the KM and LM cases do not show significant differences, only the latter will be described in detail in what follows.

Figure 6 compares the measured and computed turbulent kinetic energy profiles at several stations starting from the separation point. The agreement between computations is generally satisfactory, even though the models overpredict the turbulent kinetic energy in the backflow region. Of the two, version (2) of the model seems to reduce the overprediction. This was also found in the high Reynolds number case. This overprediction spreads in the shear layer as the flow proceeds downstream.

The overprediction of k seems to have an effect in terms of turbulent shear stress also, as shown in Fig. 7. Here the turbulent shear stress is overestimated by both the formulations in the backflow region and underestimated in the recovery region. The change from overestimation to underestimation takes place gradually across the reattachment point and the fit between DNS and computations improves only far downstream.

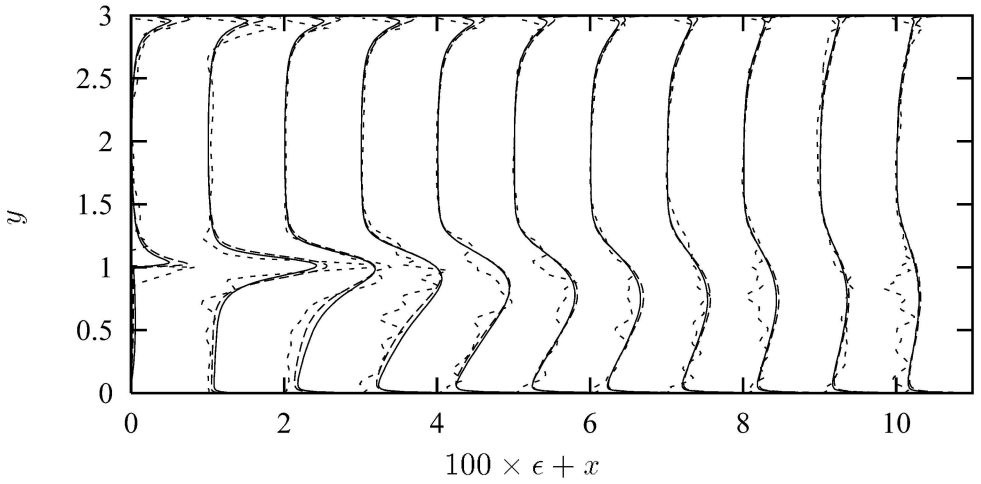

FIGURE 8. *LM* Dissipation rate profiles. Symbols as in Fig. 4.

The *LM* data set also includes the dissipation rate. Figure 8 shows that the computed dissipation rate level is larger than that given by the DNS in the backflow region. The ϵ levels are well predicted in the recovery region.

The skin friction coefficients in Figs. 9 and 10 show that version (2) of the model tends to reduce the recirculation bubble length in the low-Re number case (a similar trend was also found for the KM test), whereas the same model seems to increase the backflow region length in the high-Re case. In the KM case, also, a reduction of the recirculation bubble length was observed.

4. Discussion and conclusions

The brief description of the computations done in the previous section evidences how the computed overall flow pattern agrees with the high-Re and low-Re cases, although some discrepancies between the computations and the measurements (and DNS) arise in terms of turbulence quantities.

In the recovery region, as already pointed out by several authors, (*e.g.* Durbin, 1995), the computations recover to a boundary layer profile much more slowly than experiments would indicate at high Reynolds numbers. This disagreement fades away for smaller Reynolds numbers, as those typical of the DNS. In the backflow region the computed profiles seem too steep, which would indicate too large a turbulence level.

Version (2) of the model was found to work slightly better than the original version of the model in the backflow region. This can be attributed to the different choice of the length scale formula. In version (1) the model chooses between two different values of the length scale, whereas in version (2) the expression for the length scale allows a smooth switch from the two values. Observe that the same smooth switch is guaranteed for the computation of the time scale. This seems to play a significant role in the improvement of the results where, due to the small local Reynolds number, the expressions for the length and time scale are switching between the two values. In the recovery region the local Reynolds number is larger

and the beneficial effects of the smooth transition between the two values of the time and length scale formulas disappear.

In terms of turbulent shear stress, the backflow region again shows some slight inaccuracies for both the high-Re and low-Re cases. This fits with the shape of the computed velocity profile, which indicates that the mean velocity gradient and the turbulence levels are too high. From the DNS data set it is possible to compute a turbulent viscosity μ_t via the definition of the turbulent shear stress given in the Boussinesq assumption. This sort of computation does not guarantee that the turbulent viscosity is positive, since there is no guarantee that the mean shear and the turbulent shear stress always have opposite sign: in fact Fig. 11 shows that turbulent viscosity computed from the turbulent shear stress by DNS gives negative values.

The turbulent viscosity is small deep inside the backflow region and grows toward the reattachment point. The two versions of the model are found to overestimate the turbulent viscosity in the backflow region. There is very little difference between the computations all through the computational domain. Observe that a large turbulent viscosity would imply a large momentum diffusion, which should decrease the recirculation bubble length. Surprisingly, this is not the case in the computations: the overestimation in μ_t is followed by an excellent agreement between the computed and measured reattachment point. The figure also shows that the disagreement between the computations and the DNS fades away downstream of the reattachment point. But the same figure also shows that in the recovery region the turbulent viscosity is underestimated. The smaller momentum diffusion in the computation could partially explain why the computed velocity profiles tend to the boundary layer profiles too slowly. The discrepancies between DNS and computations are mainly in the backflow region and the shear layer, since above the latter the computations seem to follow the DNS profiles quite well.

The DNS data set also contains all the terms of the transport equation for the turbulent kinetic energy. With these data it was possible to evaluate the accuracy of each term of the modeled transport equation for k. A full comparison of all the terms (*i.e.* convection= C_k, viscous diffusion= Vd, turbulent diffusion= Td, pressure diffusion= Pd, production= P_k, and dissipation= ϵ) showed that the viscous diffusion Vd has nearly no effect. The computed convection of k, C_k, is in very good agreement with both the measurements by KM and the DNS by LM. The dissipation rate, although not in perfect agreement with the data in the backflow region, closely resembles the DNS profiles in the shear layer. So, the terms which need a further check, and that are not often compared with the experiments for models based on the eddy viscosity, are the production rate P_k and both the turbulent and pressure diffusion terms Td and Pd respectively.

Figure 12 compares the DNS production rate versus the profiles obtained by using the two different versions of the model. The agreement between computations and the DNS profiles is good. Observe that the peak in the production rate, which is probably caused by the very high mean shear downstream of the separation point, is well captured. The production rate is somewhat overpredicted in the backflow

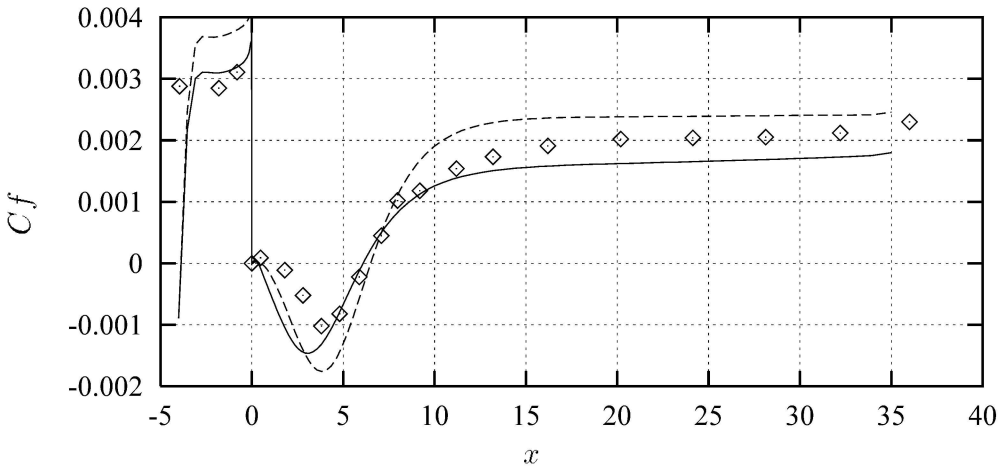

FIGURE 9. *DS* Skin friction coefficient. ◇ experiments, —— model version (1), – – – model version (2).

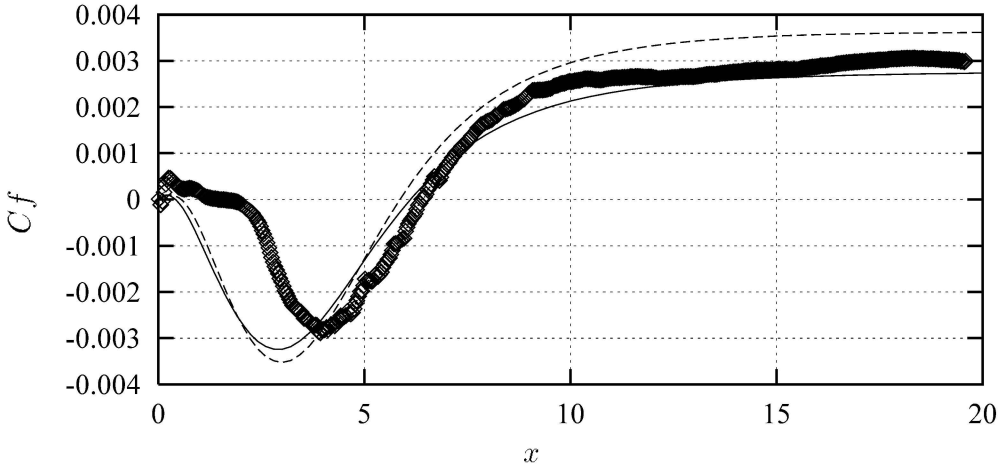

FIGURE 10. *LM* Skin friction coefficient. Symbols as in Fig. 9.

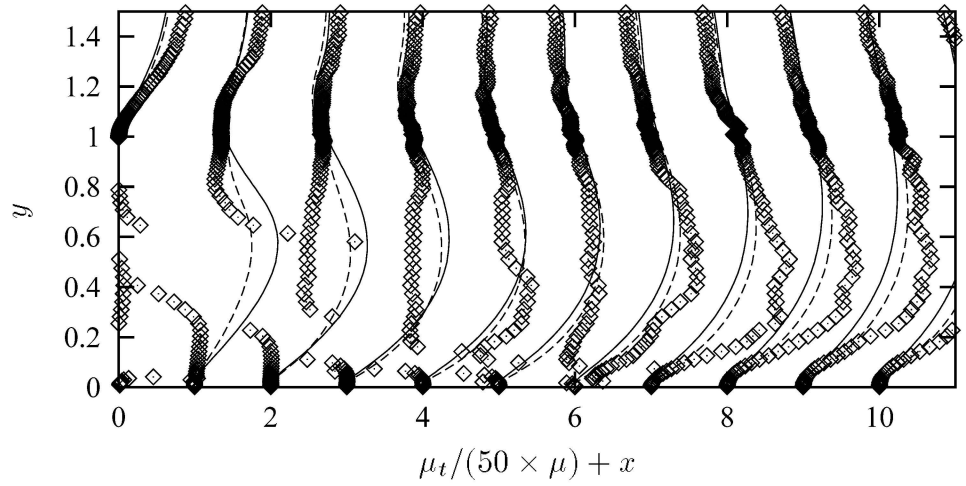

FIGURE 11. *LM* Turbulent viscosity profiles. Symbols as in Fig. 9.

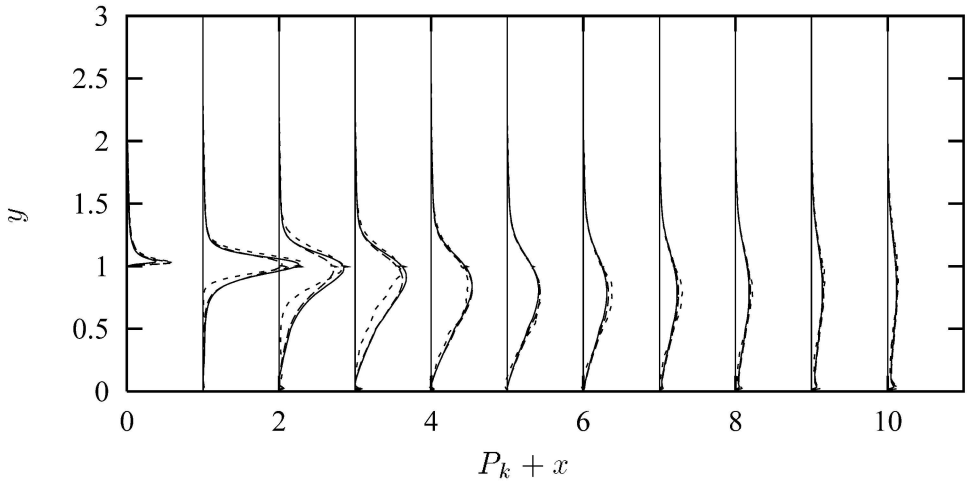

FIGURE 12. *LM* Production rate profiles. ---- experiments, —— model version (1), ——— model version (2).

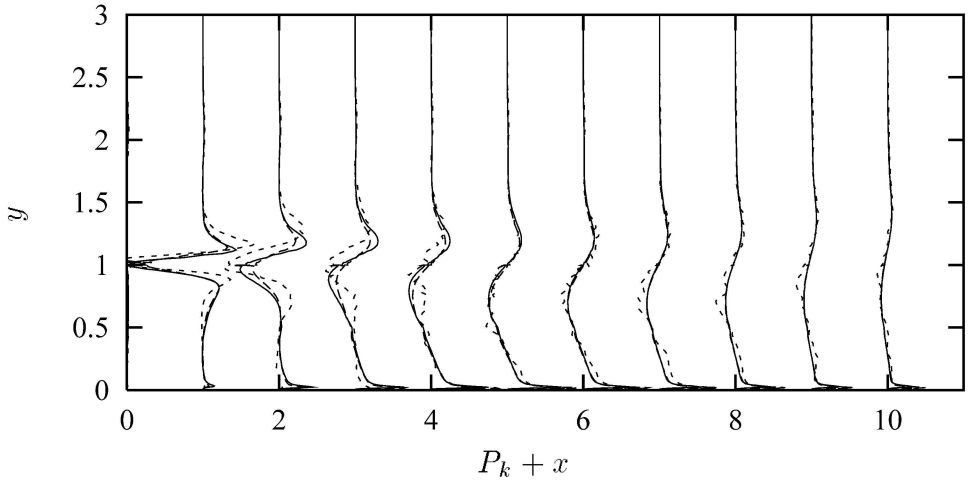

FIGURE 13. *LM* $Td + Pd$ profiles. Symbols as in Fig. 12.

region, but this overprediction seems to fade away as the reattachment point is reached. The same agreement was found in the high-Re case.

Before comparing the turbulent and pressure diffusion terms, one should recall that the gradient diffusion hypothesis, done in the $k-\epsilon$ model, does not distinguish between Pd and Td, which are just lumped together. Still, it is possible to compare the sum of Td and Pd from the DNS calculations with the computed turbulent diffusion of turbulent kinetic energy, which should be the sum of the two. Observe that the comparison is done for the diffusive terms (second order derivative of k for the $k-\epsilon$ model and first order derivative of Td and Pd for the DNS data). Figure 13 compares the computed diffusion of k with the sum of the turbulent diffusion and pressure diffusion from the DNS. The agreement between computations and DNS is quite good. The up-down shape of the profile from the DNS is closely reproduced by the calculations. The agreement remains good in the entire computational domain and does not deteriorate when making the same comparison for the KM data set.

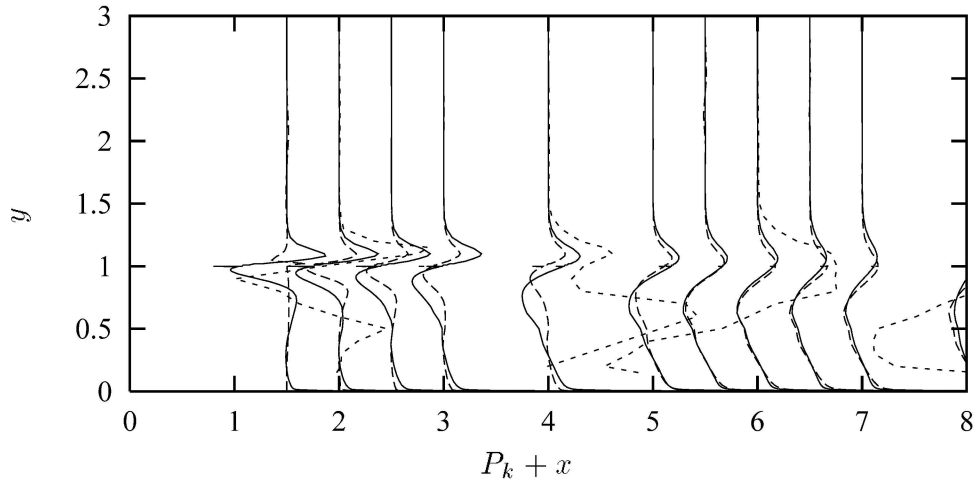

FIGURE 14. *DS Td* profiles. Symbols as in Fig. 12.

When making the same comparison by using the *DS* data base at a higher Reynolds number, some problems arise due to the scatter of the measured data. Figure 14 compares the turbulent diffusion of turbulent kinetic energy for the *DS* case. Although there are not as many data as in the DNS case, the figure clearly suggests that the turbulent diffusion is largely underestimated in the shear layer from the separation point till far downstream. The underestimation is quite severe and clearly limited to the flow region where the mean shear is high. However, the experimental data are probably not accurate enough to differentiate, as in Fig. 14.

Figures 13 and 14 indicate that as long as the Reynolds number is small, the gradient diffusion hypothesis gives the correct estimate of the turbulent plus the pressure diffusion, especially in the high shear layer. The two figures also show that the same closure hypothesis fails when the Reynolds number is large. Apparently at large Re there is a large scatter of turbulence time and length scales. This scatter is probably not modeled when using a linear eddy viscosity model. The scatter is reduced at smaller Reynolds number, and the turbulence model then agrees much better with the experiments and DNS.

In conclusion, the computations show that the slow recovery downstream of the reattachment point occurs only in high Reynolds number flows and is probably caused by the gradient diffusion hypothesis, which is not able to model the large turbulent diffusion typical of the high shear layer. In the backflow region the computations and the comparison with the experiments and the DNS do not allow identification of any specific deficiency of the model. Still, the plots indicate that in the backflow region the models predict too high a turbulence level and too much velocity gradient, which are interrelated deficiencies.

Acknowledgements

The first author would like to express his gratitude to CTR, and the Energetics Department of the University of Genova, Italy, for their financial support.

REFERENCES

Driver, D., & Seegmiller, H. L. 1985 Features of Reattaching Turbulent Shear Layer in Divergent Channel Flow. *AIAA J.* **23,** 162-171.

Durbin, P. A. 1995 Separated flow computations with the $k-\varepsilon-\overline{v^2}$ model. *AIAA J.* **33,** 659-664.

Durbin, P. A. & Laurence, D. 1996 Non-local effects in single point closure. *Advances in Turbulence Research,* Seoul, Korea, May 17, 1996, 109-120.

Kasagi, N., & Matsunaga, A. 1995 Three-dimensional particle-tracking velocimetry measurements of turbulence statistics and energy budget in a backward-facing step flow. *Int. J. Heat and Fluid Flow.* **16,** 477-485.

Le, H., & Moin, P. 1994 Direct numerical simulation of turbulent flow over a backward facing step. *Report TF-58,* Thermosciences Division, Department of Mechanical Engineering, Stanford University.

Michelassi, V. 1993 Adverse pressure gradient flow computation by two-equation turbulence models. *Engineering Turbulence Modeling and Experiments.* **2,** W. Rodi & F. Martelli (ed.) 123-132.

Michelassi, V., Rodi, W.,& Giess, P.-A. 1997 Experimental and numerical investigation of boundary-layer and wake development in a transonic turbine cascade. *IGTI Conference,* Orlando, FL.

Michelassi, V., & Shih, T. H. 1991 Low Reynolds Number Two-Equation Modeling of Turbulent Flows. *NASA TM-104368.*

Michelassi, V., Theodoridis, G., & Papanicolaou, E. 1995 A Comparison of Time Marching and Pressure Correction Algorithms for Transonic Turbine blades. *ASME AD.* **49,** 115-126.

Rodi, W. 1991 Experience with two-layer models combining the $k-\epsilon$ model with a one-equation model near the wall. *AIAA-91-0216.*

Rodi, W., Bonnin, J.-C., & Buchal, T. (ed.) 1995 Proceedings of the ERCOFTAC Workshop on data bases and testing of calculation methods for turbulent flows. *University of Karlsruhe, Germany.*

Rodi, W., & Mansour, N. N. 1990 Low Reynolds number $k-\epsilon$ modeling with the aid of direct simulation data. *Proceedings of the Summer Program.* Center for Turbulence Research, NASA Ames/Stanford Univ. 85-106.

Rodi, W., Mansour, N. N., & Michelassi, V. 1993 One-equation near-wall modelling with the aid of direct simulation data. *ASME Journal of Fluids Engineering.* **115,** 196-205.

Zhu, J., & Shih, T. H. 1993 Calculations of Turbulent Separated Flows. *NASA TM-106154.*